Physics and Imaging in Radiation Oncology 31 (2024) 100609

Contents lists available at ScienceDirect

Physics and Imaging in Radiation Oncology

journal homepage: www.sciencedirect.com/journal/physics-and-imaging-in-radiation-oncology

Original Research Article

Motion-induced dose perturbations in photon radiotherapy and proton therapy measured by deformable liver-shaped 3D dosimeters in an anthropomorphic phantom

Simon Vindbæk [a,b,*], Stefanie Ehrbar [c], Esben Worm [d], Ludvig Muren [a,b], Stephanie Tanadini-Lang [c], Jørgen Petersen [b,d], Peter Balling [e,f], Per Poulsen [a,b]

[a] Danish Centre for Particle Therapy, Aarhus University Hospital, Aarhus, Denmark
[b] Department of Clinical Medicine, Aarhus University, Aarhus, Denmark
[c] Department of Radiation Oncology, University Hospital Zürich and University of Zürich, Zürich, Switzerland
[d] Department of Medical Physics, Aarhus University Hospital, Aarhus, Denmark
[e] Department of Physics and Astronomy, Aarhus University, Aarhus, Denmark
[f] Interdisciplinary Nanoscience Center, Aarhus University, Aarhus, Denmark

ARTICLE INFO

Keywords:
3D dosimetry
Deformable phantom
Gating
Radiotherapy
Proton therapy
Anthropomorphic
Motion management

ABSTRACT

Background and purpose: The impact of intrafractional motion and deformations on clinical radiotherapy delivery has so far only been investigated by simulations as well as point and planar dose measurements. The aim of this study was to combine anthropomorphic 3D dosimetry with a deformable abdominal phantom to measure the influence of intra-fractional motion and gating in photon radiotherapy and evaluate the applicability in proton therapy.
Material and methods: An abdominal phantom was modified to hold a deformable anthropomorphic 3D dosimeter shaped as a human liver. A liver-specific photon radiotherapy and a proton pencil beam scanning therapy plan were delivered to the phantom without motion as well as with 12 mm sinusoidal motion while using either no respiratory gating or respiratory gating.
Results: Using the stationary irradiation as reference the local 3 %/2 mm 3D gamma index pass rate of the motion experiments in the planning target volume (PTV) was above 97 % (photon) and 78 % (proton) with gating whereas it was below 74 % (photon) and 45 % (proton) without gating.
Conclusions: For the first time a high-resolution deformable anthropomorphic 3D dosimeter embedded in a deformable abdominal phantom was applied for experimental validation of both photon and proton treatments of targets exhibiting respiratory motion. It was experimentally shown that gating improves dose coverage and the geometrical accuracy for both photon radiotherapy and proton therapy.

1. Introduction

Intra-fractional motion of abdominal or thoracic tumours can compromise the treatment delivery. Specifically, liver tumours can rotate [1,2], deform [3], or move several centimetres with respiration [1,4–6], which can result in dose perturbations such as blurring and shifted doses [7]. For dynamic treatments such as pencil beam scanning proton therapy, the simultaneous beam and tumour motion can lead to interplay effects [8–13] with hot and cold spots in or near the target region. Motion mitigation strategies are important in radiotherapy to account for internal organ motion and include a planning margin in the planning target volume, respiratory gating [14], breath-hold [15], image tracking [16,17] e.g. combined with gold fiducial markers [18,19], or repainting in proton therapy. These strategies may reduce the effects of intra-fractional motion and help to maintain target coverage.

The effects of gating in photon radiotherapy and proton therapy have been simulated [20–22] and dose reconstructed [23]. However, experimentally for proton therapy, these investigations have been limited to point [24,25] and planar [26,27] measurements. Progression in three-dimensional (3D) dosimetry has led to both deformable [28–30] and anthropomorphic [31] 3D dosimeters that are applicable for both

* Corresponding author at: Danish Centre for Particle Therapy, Aarhus University Hospital, Aarhus, Denmark.
E-mail address: sivije@rm.dk (S. Vindbæk).

https://doi.org/10.1016/j.phro.2024.100609
Received 28 February 2024; Received in revised form 23 June 2024; Accepted 1 July 2024
Available online 6 July 2024

photon and proton therapy [32–35]. Combining deformable anthropomorphic 3D dosimeters with anthropomorphic motion phantoms has the potential to evaluate the efficacy of e.g. gating and repainting in terms of maintaining target coverage in proton therapy of moving tumours.

The aim of this study was therefore to investigate if the combination of anthropomorphic 3D dosimeters embedded in a deformable phantom can be used to measure the effects of gating on clinically relevant photon and pencil beam scanning proton therapy liver treatments.

2. Material and methods

2.1. Liver dosimeter fabrication

Two batches, each containing three liver dosimeters, were fabricated following a previously developed protocol [31]. The first batch was used for proton therapy, while the second batch was for photon radiotherapy. A 3D liver model, based on a patient computed tomography (CT) scan, was used for the liver-shaped dosimeters. The liver was divided into three smaller parts to fit each part into the optical CT scanner, used to read out the optical attenuation coefficients of the dosimeter, and to avoid too large light attenuation in the optical scanner. Silicone rubber casting moulds for each liver part were made by 3D-printing each part using polylactic acid filament which was then sanded, painted, and primed before being suspended in a 20:1 mixture of Xiameter RTV 3481 silicone rubber and Xiameter RTV 3081 curing agent and left to cure.

A highly transparent silicone kit SYLGAARD® 184 (93.2 % silicone-elastomer, 5.1 % curing agent) was mixed thoroughly with chloroform (1.5 %) and the radiosensitive material leucomalachite green (0.26 %) and poured into the silicone rubber moulds. The largest and most central liver part was cast using the dosimeter mixture whereas the two smaller parts were cast in pure silicone since they were not used for dosimetry in this study. The dosimeters were cured ventilated in the dark for 72 h.

2.2. Abdominal motion phantom

The deformable liver phantom (ELPHA) was developed by Ehrbar et al. [36] and adapted for the use of 3D dosimetry. ELPHA consisted of three parts: The liver (3D dosimeter), the soft tissue-like bottom part (abdomen) and the lung tissue-like top part (Fig. 1).

The abdominal mould of the original ELPHA was re-used to generate the same abdominal outline. A liver model was 3D-printed in one part using the 3D liver file to create a liver-shaped pocket in the abdominal phantom for the 3D dosimeter parts. Clay and the liver model were used to make negative shaped notches for the alignment of the top and bottom parts and to make an inlay for the 3D dosimeter (Fig. 1A). The soft tissue-like abdominal part (Fig. 1B) was cast first with the silicone products Ecoflex GEL and Dragon Skin (SmoothOn Inc., Macungie, PA, USA). Both are two-component silicones with platinum-based cure systems. These silicones were initially designed for silicone prosthetic appliances, where the softer Ecoflex is encapsulated in a layer of Dragon Skin. The bottom abdominal part and liver model were inserted again into the abdominal mould and used to mould the fitting lung part (Fig. 1C). The lung part (Fig. 1D) was cast from a mixture of Dragon Skin with polystyrene globules of 3–5 mm diameter (Granulex ultralight, GLOREX AG, Füllinsdorf, Switzerland). For easy separation of the cured abdominal parts, Ease Release 200 (SmoothOn Inc., Macungie, PA, USA) was sprayed onto the bottom abdominal part before casting the top lung-like part.

Prior to radiotherapy delivery, the three parts of the liver dosimeter were inserted into the abdominal parts (Fig. 1E) and the whole abdomen was mounted on the phantom deformation stage (Fig. 1F). The deformation stage deformed the abdomen along the superior-inferior direction, by compressing the abdomen between two hard plastic plates. One plate was stationary while the other was moving and driven by a motor. This is described in more detail in Ehrbar et al. [36].

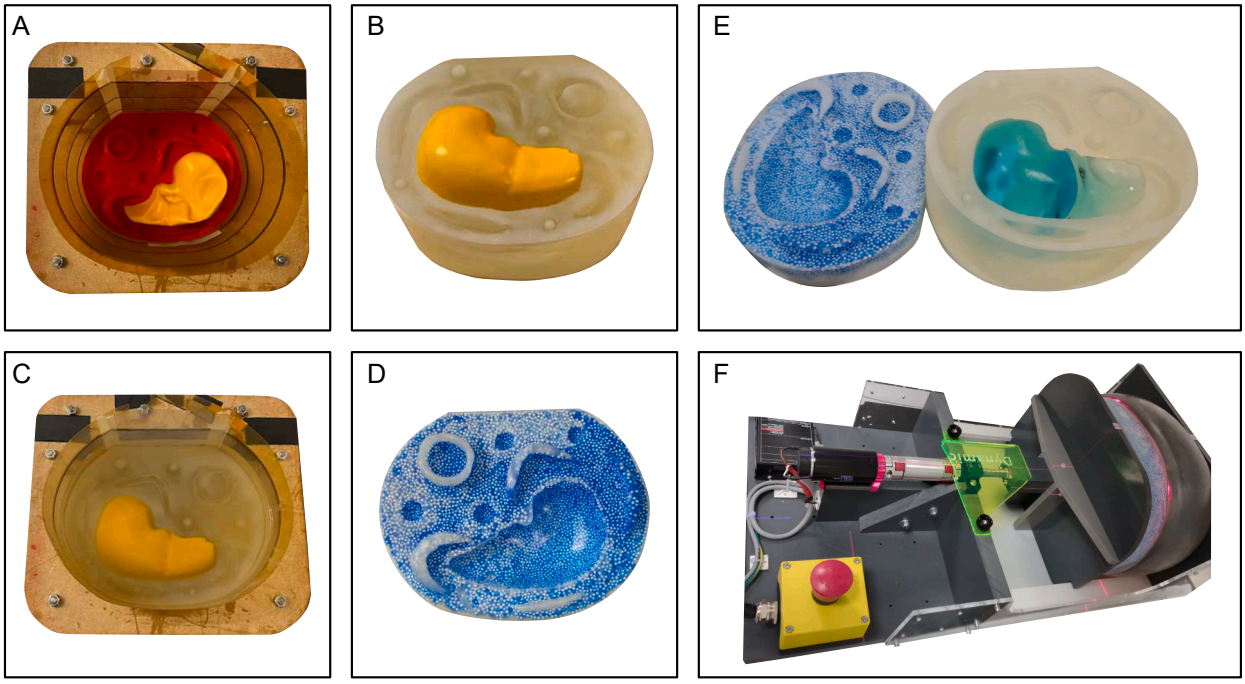

Fig. 1. A) Abdominal mould (wood and plastic foil) with clay (red) for notches and 3D-printed liver model (yellow) as a placeholder for the 3D dosimeter. **B)** Soft-tissue-like bottom part of the abdomen with the liver model. **C)** Bottom abdominal part and liver model inserted in the abdominal mould to generate the mould for the top lung-like part. **D)** Lung-like top part of the abdomen (blue). **E)** Soft tissue and lung-like parts and 3D liver dosimeter (light blue). **F)** Abdominal parts and 3D dosimeter assembled on the deformation stage. (For interpretation of the references to colour in this figure legend, the reader is referred to the web version of this article.)

2.3. 4DCT and treatment planning

The three liver parts were inserted into the abdominal phantom. Two gold markers were inserted in each of the two silicone-only liver parts for reference alignment using an implantation needle. Two additional gold markers were inserted in the abdominal phantom. A ten-phase 4DCT scan of the abdominal phantom was recorded on a Siemens CT scanner with phase binning based on the Varian Respiratory Gating for Scanners system. During the 4DCT, the motion phantom moved sinusoidally with a 12 mm peak-to-peak amplitude and a four-second period. In a study by Suh et al. the overall mean respiration period for abdominal radiotherapy patients have been found to be around 3.8 s [37]. The extent of deformation versus translation in the dosimeter was investigated in the 4DCT, which revealed that the liver dosimeter only deformed slightly about 1 mm and primarily translated almost 12 mm peak-to-peak due to its larger stiffness compared to the soft-tissue bottom part of the phantom.

The CT scan was imported into the Eclipse (version 16.1) treatment planning system (TPS; Varian Medical Systems, Palo Alto, CA, USA) and the exhale phase of the 4DCT scan was selected for treatment planning, resembling the clinical workflow for liver treatments at the Danish Centre for Particle Therapy [23]. A fictive stereotactic clinical target volume (CTV) with a volume of 8.6 cm^3 was delineated in the radiochromic liver part and used as the target volume for photon and proton treatment planning. The photon plan was a 6 MV volumetric modulated arc therapy (VMAT) plan with two arcs that each spanned 120°. A planning target volume (PTV) was constructed by adding a 3 mm isotropic margin to the CTV, and the plan was optimized to cover this PTV by the 95 % isodose. A mean CTV dose of 9 Gy was applied for the photon plan.

The proton plan was based on two intensity modulated proton therapy (IMPT) fields. No PTV was applied but the plan instead used robust multi-field optimization (MFO) including ±3 mm shifts along each axis and ±3.5 % range uncertainty (Fig. 2). The ratio of the water equivalent path length to the physical length was measured to 0.937 (abdomen) and 0.309 (lung) which translated to −90 HU (abdomen) and −673 HU (lung) in the Eclipse TPS. For proton therapy, the dosimeter's CT number was overwritten with −64 HU found in a previous study through a water equivalent path length experiment [38]. The proton plan was normalized to deliver 12 Gy per fraction as the mean dose to the CTV with CTV coverage by the 95 % isodose in all robustness scenarios. The Varian proton convolution superposition algorithm (version 16.1) was applied for the dose calculation. Furthermore, a PTV was delineated as a volume of interest for comparing the different scenarios and defined as the CTV with a 3 mm margin. Different doses were used for photon radiotherapy and proton therapy since the dosimeter response depends on the irradiation modality. For each modality, an appropriate dose was chosen to give a clearly visible signal while still avoiding too much darkening with large light attenuation in the optical scanner.

2.4. Irradiation

Irradiations were performed on a Varian TrueBeam accelerator (photons) and a Varian ProBeam gantry (protons). For both photons and protons, three scenarios were investigated. The scenarios included (1) stationary irradiation with the phantom parked in the exhale position, (2) motion with no gating, and (3) motion with gating. For the motion scenarios (2–3), the abdominal phantom moved sinusoidally with a 12 mm peak-to-peak amplitude. For each scenario, a cone-beam CT (CBCT) was recorded without phantom motion and used for image-guided setup by registration with the planning CT. The phantom was set up to slightly different positions for each irradiation scenario to obtain a clinically realistic comparison between the scenarios. For the stationary irradiation, the phantom was aligned to match the exhale phase planning scan. For the motion-including irradiations without gating, the phantom was set such that it matched the planning scan in the middle of the full motion cycle, thus resembling free-breathing treatment with setup to the mean target position. For the motion-including irradiations with gating, the phantom was setup to match the planning scan when it was in the

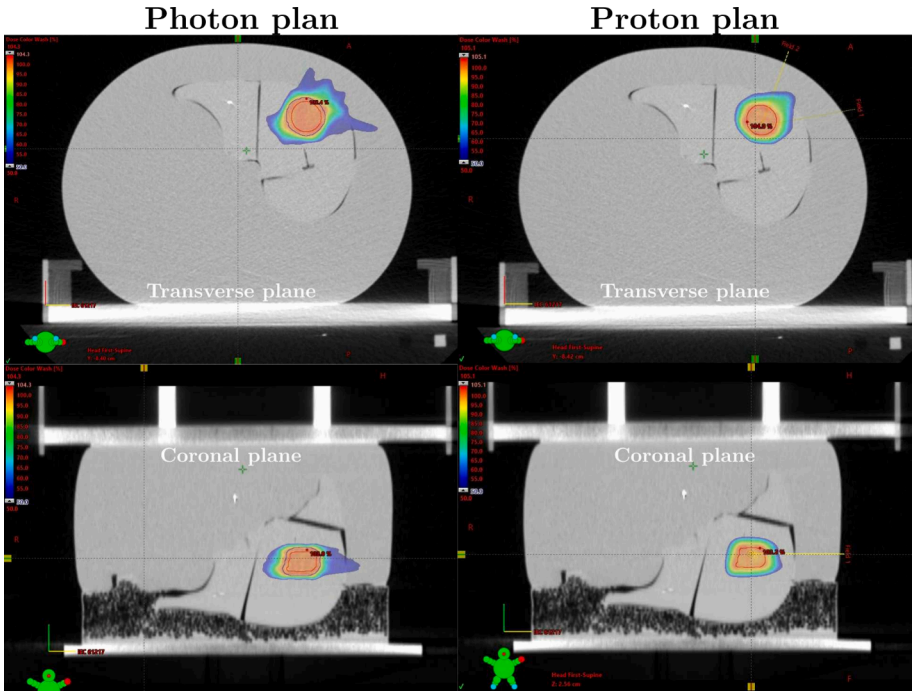

Fig. 2. CT slices of the abdominal phantom in the exhale phase showing the photon VMAT plan (left) and the proton PBS plan (right). Colorwash shows the dose in range 50–104.3 % (photon) and 50–105.1 % (proton) of the prescribed dose. The CTV is delineated in red while the PTV for the photon plan is delineated in purple. The white marks in the liver and abdomen are the gold markers. The air gaps in the liver show where the liver parts separate. (For interpretation of the references to colour in this figure legend, the reader is referred to the web version of this article.)

mid-position of the gating window.

The gated irradiations were guided by a standard Varian gating marker block positioned on top of the phantom using the integrated TrueBeam gating system (photons) or the Varian RPM gating system (Protons). Gating windows were set such that irradiation occurred with a duty cycle of 34 % around the exhale phase.

2.5. Dosimeter read-out and data analysis

The dosimeters were read out pre- and post-irradiation using a Vista™ 16 optical CT scanner. The post-irradiation scans began an hour after the final irradiation. For 3D reconstruction of the optical signal, the ordered subset convex total variation algorithm [39] was applied using 2000 projections resulting in 1 mm^3 voxels. The quantity measured by the optical CT was not dose but rather the change in attenuation coefficients $\Delta\alpha$. For a photon irradiation, $\Delta\alpha$ is proportional to dose, meaning $\Delta\alpha$ and photon dose are interchangeable. For a proton irradiation, $\Delta\alpha$ is also proportional to dose but in addition has an exponential dependency on both linear energy transfer (LET) and dose rate [34,31]. Converting the linear attenuation coefficients to dose for protons is time-consuming and requires a LET calculation on the moving phantom which was not considered feasible. Instead, $\Delta\alpha$ was compared directly for both photon and proton irradiations to investigate the ability of a simple workflow to assess the impact of motion and gating on the delivered dose.

A boolean mask of the liver was created for each of the measured 3D $\Delta\alpha$ distributions, and for each batch they were aligned to the stationary scenario using the image registration function `imregtform` in Matlab. Global and local 3D 3 %/2 mm and 5 %/2 mm gamma index analyses were applied to compare the experimental measurements for the CTV and PTV using the stationary measurements as the reference. A global gamma index analysis uses ± the set percentage of the global maximum $\Delta\alpha$ value whereas local refers to the local $\Delta\alpha$ value of the given voxel which makes the local gamma index analysis more strict. Furthermore, the mean percentage difference in the CTV and PTV were calculated as $\text{mean difference}(\%) = \frac{\text{mean}(\Delta\alpha_{Motion} - \Delta\alpha_{Ref})}{\max(\Delta\alpha_{Ref})} \cdot 100$ using boolean masks as well as the standard deviation.

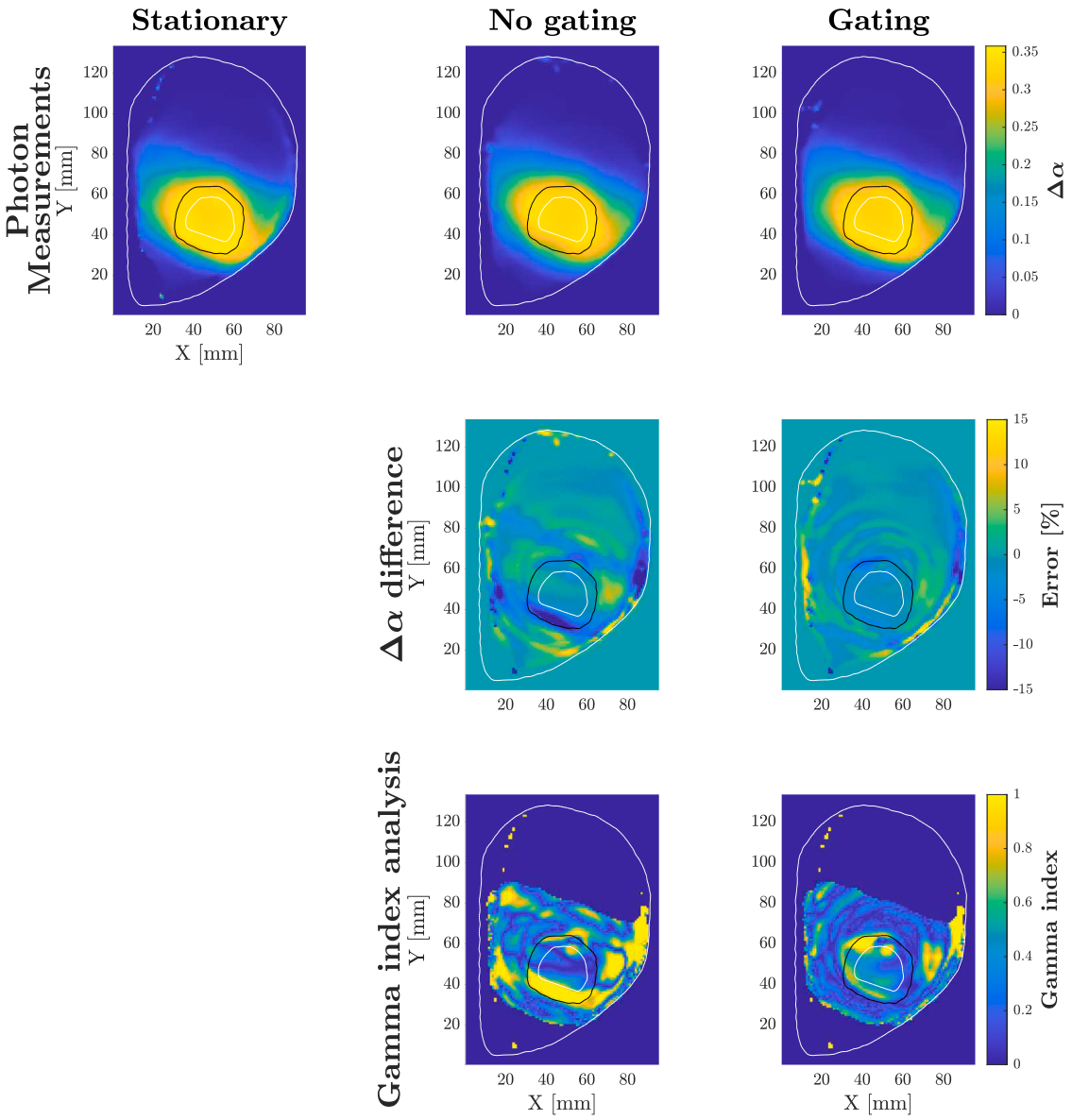

Fig. 3. Slices of the photon $\Delta\alpha$ measurements (first row), the $\Delta\alpha$ difference between the motion scenarios and the stationary experiment in terms of % of $\max(\Delta\alpha_{Ref})$ (second row), and the 3 %/2 mm gamma index calculated in voxels at or above 10 % of $\max(\Delta\alpha_{Ref})$. The white inner contour is the CTV, the black contour is the PTV, and the white outer contour is the liver outline.

Furthermore, volume histograms of the $\Delta\alpha$ distributions were made to compare the target coverage in each measurement. Although $\Delta\alpha$ corresponds to the dose in photon therapy and has a LET and dose rate dependency in proton therapy, the same analysis was performed for the two irradiation modalities.

3. Results

There were small differences between the motion-including experiments and the stationary measurement when gating was applied but notable differences without gating for both photon (Fig. 3) and proton therapy (Fig. 4). Gating, non-surprisingly, ensured a better dose coverage for photon therapy and had a better agreement in $\Delta\alpha$ coverage for proton therapy.

The gamma index analysis (Table 1) revealed that the local and global 3 %/2 mm and 5 %/2 mm gamma index pass rates for gating in photon therapy remained above 96 % in both the CTV and PTV whereas for no gating it ranged from 73 % to 84 %. This difference in gamma index pass rates was supported by the mean difference being lower for gating than for no gating. Overall the gamma pass rates for proton

Table 1
Gamma index analysis pass rates (first four rows) for two criteria (3 %/2 mm/5 %/2 mm) are included for all motion-including experiments. Also, the mean $\Delta\alpha$ difference (last row) between the stationary measurement and the different motion experiments are included in % ± the standard deviation normalized to $\max(\Delta\alpha_{Ref})$ for both the (CTV/PTV) regions.

Gamma index analysis (5 %/2 mm/3 %/2 mm)				
Volume region	Photon no gating	Photon gating	Proton no gating	Proton gating
CTV (global) [%]	84.3/76.2	99.4/97.7	60.7/31.1	95.0/73.4
PTV (global) [%]	83.5/76.8	99.7/98.7	67.6/49.7	95.5/83.3
CTV (local) [%]	81.4/73.3	99.0/96.8	43.0/24.2	83.5/65.5
PTV (local) [%]	80.0/73.9	98.8/97.3	55.6/44.4	88.8/78.8
mean $\Delta\alpha$ difference (CTV/PTV) [%]	−1.8 ± 3.6/ −4.2 ± 6.1	−0.4 ± 1.2/ −1.0 ± 2.4	−5.5 ± 2.6/ −6.2 ± 5.0	1.6 ± 2.9/ 0.7 ± 4.3

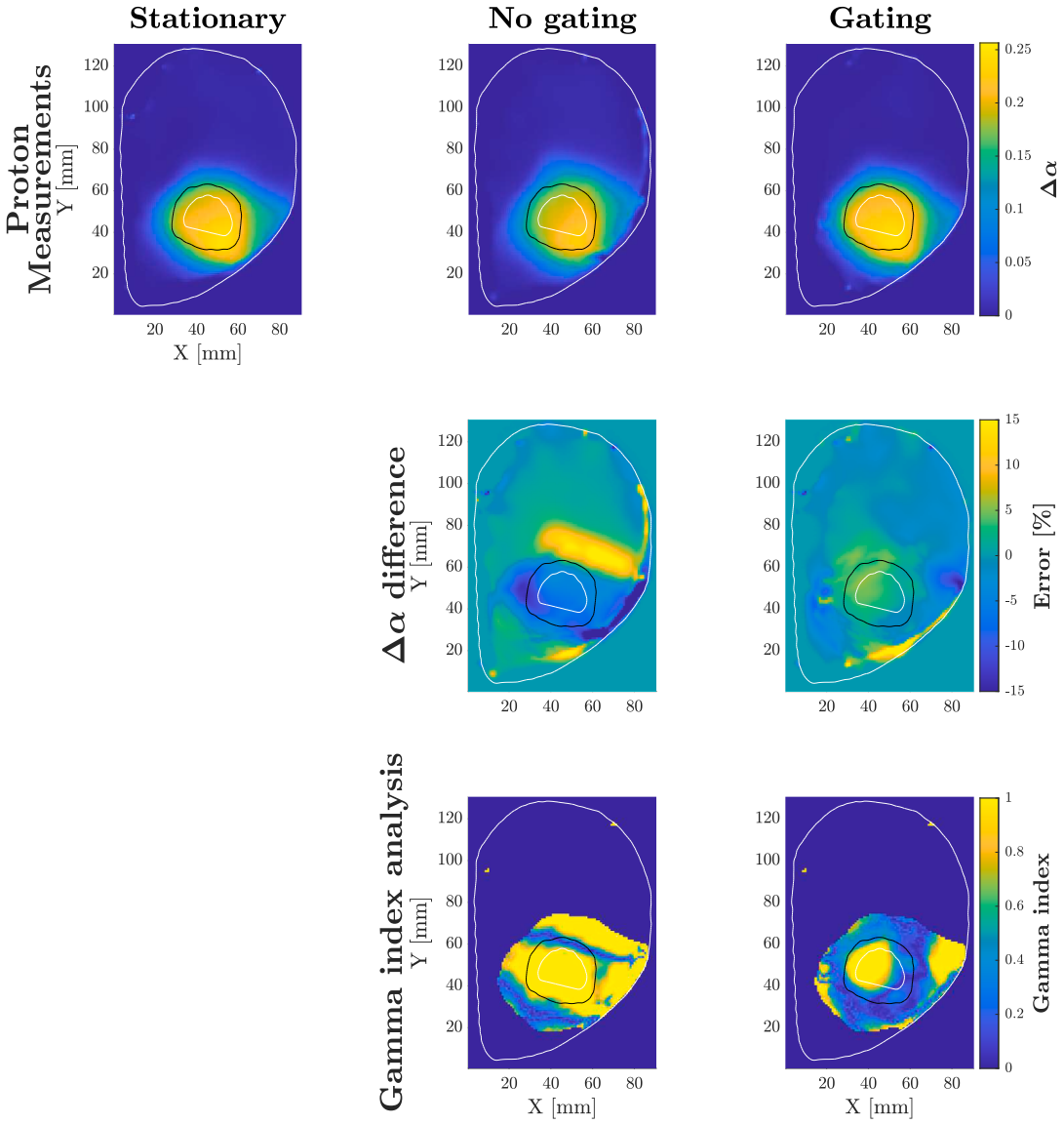

Fig. 4. Slices of the proton $\Delta\alpha$ measurements (first row), the $\Delta\alpha$ difference between the motion scenarios and the stationary experiment in terms of % of $\max(\Delta\alpha_{Ref})$ (second row), and the 3 %/2 mm gamma index calculated in voxels at or above 10 % of $\max(\Delta\alpha_{Ref})$. The white inner contour is the CTV, the black contour is the PTV, and the white outer contour is the liver outline.

therapy with gating ranged from 66 % (local 3 %/2 mm, CTV) to 96 % (global 5 %/2 mm, PTV). Without gating the gamma index pass rate fell to between 24 % (local 3 %/2 mm, CTV) and 68 % (global 5 %/2 mm, PTV). The spread for the mean $\Delta\alpha$ difference for photon therapy without gating was about three times higher as with gating whereas for proton therapy the spread was similar with and without gating. The distributions of $\Delta\alpha$ differences between motion and stationary experiments (Fig. 5) had many underdosed voxels without gating for photon therapy while maintaining a peak near zero percent difference. For proton therapy, the mean difference was shifted downwards by about 5–6 percent for motion without gating compared to the stationary experiment.

In the $\Delta\alpha$ volume histogram (Fig. 5), the stationary and gated photon irradiation had a very similar coverage for both the CTV and PTV, whereas motion without gating resulted in a clear underdosage of both the CTV and PTV. This was also the case for the proton measurements but here the gated measurement had a slightly larger signal than the stationary measurement.

4. Discussion

In this study, we have established and applied a method for

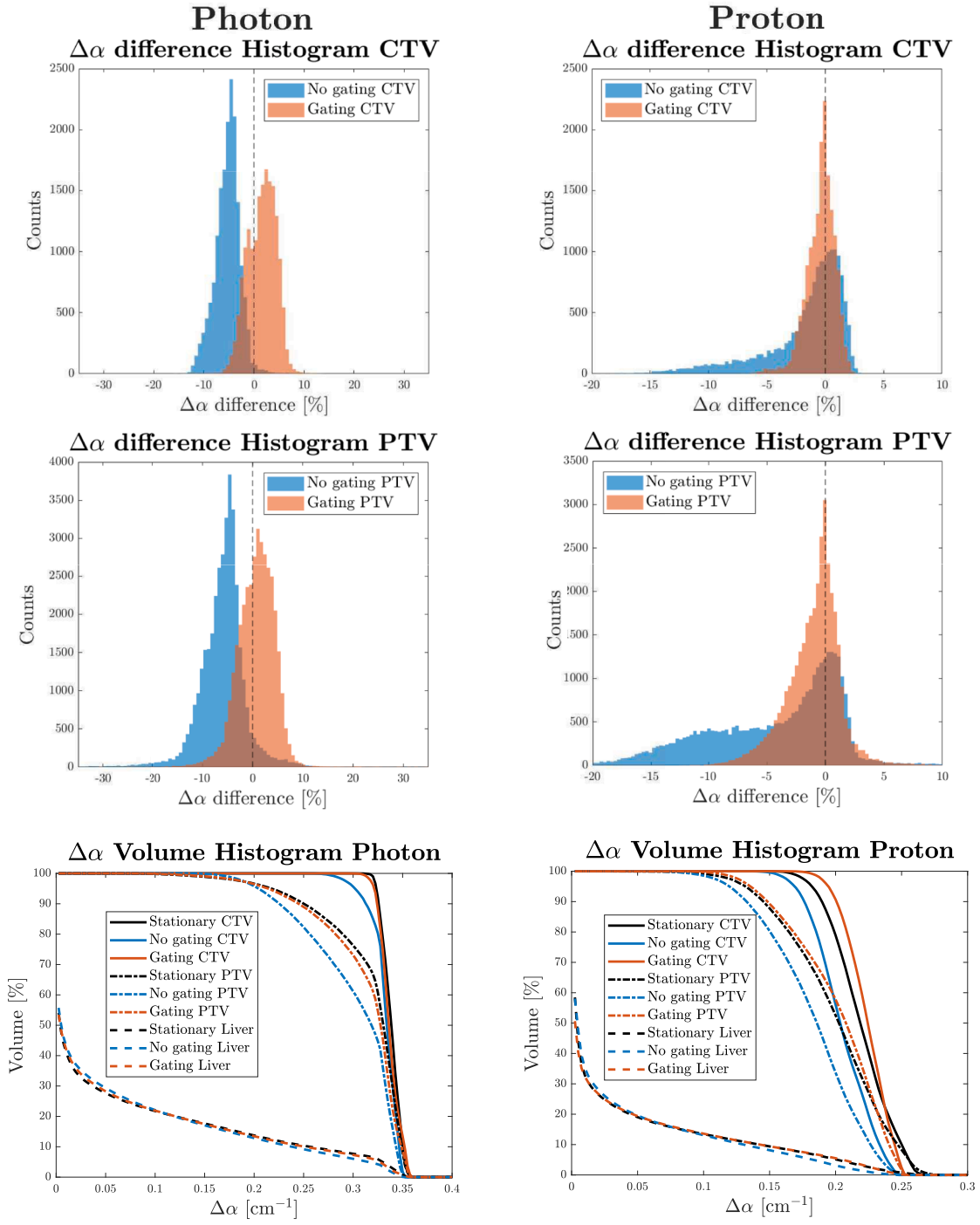

Fig. 5. Histogram of the $\Delta\alpha$ difference between the motion and stationary irradiations normalized to $\max(\Delta\alpha_{Ref})$ for both the CTV and PTV and the $\Delta\alpha$ volume histograms of the different measurements for the CTV, PTV, and the entire liver dosimeter for both the photon (left column) and proton (right column) irradiations.

measuring the spatial $\Delta\alpha$ distribution in a deformable radiochromic liver dosimeter embedded in an abdominal motion phantom for both photon radiotherapy and proton therapy. It allowed comparing stationary liver irradiations to gated and non-gated irradiations with motion and showed how much gating improved the dose coverage for both photon radiotherapy and proton therapy.

The global and local gamma index analysis (Table 1) and $\Delta\alpha$ histograms clearly showed the dosimetric advantage and improved dosimetric accuracy on the target volume when applying gating during both photon and proton radiotherapy. Specifically, many voxels were underdosed in the photon irradiation when no gating was applied. The $\Delta\alpha$ metric is a meaningful surrogate for dose when using photons as it is proportional to dose and is dose rate independent [32]. However, for proton therapy the $\Delta\alpha$ and dose comparison has a limitation since the signal response quenches due to dose rate and linear energy transfer. Therefore, $\Delta\alpha$ is not proportional to dose as with photons. Previously, a dose rate and LET calibration model has been applied to similar motion including experiments using a simpler non-anthropomorphic phantom but this led to overfitting [35] due to the calibration model's dependence on how the Monte Carlo simulations were performed. The issue lies primarily at the distal end of the proton fields where the LET is high (above 3 keV/μm). The spatial positioning of the deposited dose is on the other hand still represented by the proton measurements when the different dosimeters receive the same plan and dose rate. Therefore, a stationary control irradiation is useful.

The calculated target dose based on a 4DCT scan may not reflect the delivered dose in a patient due to motion variability even without considering deformation [40]. However, a simulation study investigated dose accumulation in real-time-image gated PBS proton therapy and found under-coverage for the tumour [41]. Using the experimental setup established in this paper could help validate which type of motion mitigation is necessary to relieve that problem. The abdominal motion phantom allows for patient-specific movements and thereby experimentally validating treatments where the motion is of concern. Furthermore, the liver deformation was minor around 1 mm but not too far from clinically observed breathing induced liver deformations of around 2–3 mm [42].

The CBCTs before each experiment showed that the liver dosimeter positioning in the abdominal phantom varied between the different irradiations and perfect alignment of both gold markers in the liver dosimeter was not possible. Also, the small air gaps between and around the three liver dosimeter parts which are visible in the CT scan (Fig. 2) changed position each time it was set up. Furthermore, having two identical static control experiments for each batch, e.g. two stationary irradiation, would have been advantageous as it might reveal more information about the intra-batch uncertainty. Note that in the present paper, identical treatment plans were used for gated and non-gated treatment in order to simplify the dosimetric comparisons and small treatment margins where applied in order to demonstrate the applicability of the 3D dosimetry to reveal dosimetric consequences of inadequate motion management. For even more clinically realistic scenarios, margins would typically have to be larger (especially for non-gated treatment) in order to also handle patient rotations, anatomical changes, baseline-drifts etc. which are beyond the scope of this paper.

Previously another deformable abdominal phantom has been used to validate real-time image guidance in radiotherapy with photon beams [43] and found static and gated measurements matched well compared to the non-gated measurements as we also found in this study. However, that system did not contain anthropomorphic dosimeters and it was not applicable to proton therapy. With that said, the investigated dosimetry system can be useful for photon irradiations and has a straightforward interpretation whereas for proton irradiations it has a limited scope and requires overcoming the dose-rate and LET obstacles for sensible use. A full LET and dose rate calibration could in principle be performed but it requires exact knowledge of the motion synchronized with the beam delivery and would be batch-dependent. If conducting such calibration the results would be too dependent on the simulations to reveal more information then already present without the calibration.

Future studies using the developed system could investigate motion with greater amplitudes, patient-specific movements, or deformation to a larger degree. Such measurements could potentially be used to verify the 4D dose accumulation that in recent years has been applied in radiotherapy even though it has been reported that 4D dose accumulation based on deformable image registration may hold large dosimetric uncertainties [44]. In general, there is presently a lack of experimental methods to validate computational methods in 3D and 4D despite the methods being used clinically.

In conclusion, we have developed and made the first demonstration of a high-resolution 3D liver dosimeter embedded in an anthropomorphic deformable phantom for experimental validation of both photon and proton treatments of targets that exhibit respiratory motion. The system showed experimentally that motion mitigation improves tumour coverage and geometrical accuracy when treatments are prone to intrafractional motion.

Funding

The research project was funded by the Novo Nordisk Foundation (Grant No. NNF18OC0034718) and by the Independent Research Fund Denmark (DFF), Grant No. 10.46540/3101-00053B.

Data availability statement

The data that support the findings of this study are available from the corresponding author upon reasonable request.

CRediT authorship contribution statement

Simon Vindbæk: Data curation, Formal analysis, Investigation, Methodology, Resources, Software, Validation, Visualization, Writing – original draft, Writing – review & editing. **Stefanie Ehrbar:** Conceptualization, Investigation, Methodology, Resources, Software, Writing – review & editing. **Esben Worm:** Conceptualization, Investigation, Methodology, Resources, Software, Writing – review & editing. **Ludvig Muren:** Conceptualization, Funding acquisition, Methodology, Project administration, Supervision, Writing – review & editing. **Stephanie Tanadini-Lang:** Conceptualization, Writing – review & editing. **Jørgen Petersen:** Conceptualization, Funding acquisition, Methodology, Project administration, Supervision, Writing – review & editing. **Peter Balling:** Conceptualization, Funding acquisition, Methodology, Project administration, Supervision, Writing – review & editing. **Per Poulsen:** Conceptualization, Funding acquisition, Investigation, Methodology, Project administration, Resources, Software, Supervision, Validation, Writing – review & editing.

Declaration of competing interest

The authors declare that they have no known competing financial interests or personal relationships that could have appeared to influence the work reported in this paper.

Acknowledgement

We thank Maiken Guldberg and the local Varian ProBeam team at the Danish Centre for Particle Therapy for their assistance.

References

[1] Xu Q, Hanna G, Grimm J, Kubicek G, Pahlajani N, Asbell S, et al. Quantifying rigid and nonrigid motion of liver tumors during stereotactic body radiation therapy. Int J Radiat Oncol Biol Phys 2014;90:94–101. https://doi.org/10.1016/j.ijrobp.2014.05.007.

[2] Bertholet J, Worm ES, Fledelius W, Høyer M, Poulsen PR. Time-resolved intrafraction target translations and rotations during stereotactic liver radiation therapy: implications for marker-based localization accuracy. Int J Radiat Oncol Biol Phys 2016;95:802–9. https://doi.org/10.1016/j.ijrobp.2016.01.033.
[3] Eccles CL, Dawson LA, Moseley JL, Brock KK. Interfraction liver shape variability and impact on GTV position during liver stereotactic radiotherapy using abdominal compression. Int J Radiat Oncol Biol Phys 2011;80:938–46. https://doi.org/10.1016/j.ijrobp.2010.08.003.
[4] Case RB, Sonke JJ, Moseley DJ, Kim J, Brock KK, Dawson LA. Inter- and intrafraction variability in liver position in non–breath-hold stereotactic body radiotherapy. Int J Radiat Oncol Biol Phys 2009;75:302–8. https://doi.org/10.1016/j.ijrobp.2009.03.058.
[5] Park JC, Park SH, Kim JH, Yoon SM, Song SY, Liu Z, et al. Liver motion during cone beam computed tomography guided stereotactic body radiation therapy. Med Phys 2012;39:6431–42. https://doi.org/10.1118/1.4754658.
[6] Worm ES, Høyer M, Fledelius W, Poulsen PR. Three-dimensional, time-resolved, intrafraction motion monitoring throughout stereotactic liver radiation therapy on a conventional linear accelerator. Int J Radiat Oncol Biol Phys 2013;86:190–7. https://doi.org/10.1016/j.ijrobp.2012.12.017.
[7] Worm ES, Høyer M, Hansen R, Larsen LP, Weber B, Grau C, et al. A prospective cohort study of gated stereotactic liver radiation therapy using continuous internal electromagnetic motion monitoring. Int J Radiat Oncol Biol Phys 2018;101:366–75. https://doi.org/10.1016/j.ijrobp.2018.02.010.
[8] Seco J, Robertson D, Trofimov A, Paganetti H. Breathing interplay effects during proton beam scanning: simulation and statistical analysis. Phys Med Biol 2009;54:N283–94. https://doi.org/10.1088/0031-9155/54/14/N01.
[9] Fattori G, Klimpki G, Hrbacek J, Zhang Y, Krieger M, Placidi L, et al. The dependence of interplay effects on the field scan direction in PBS proton therapy. Phys Med Biol 2019;64:095005. https://doi.org/10.1088/1361-6560/ab1150.
[10] Pakela JM, Knopf A, Dong L, Rucinski A, Zou W. Management of motion and anatomical variations in charged particle therapy: past, present, and into the future. Front Oncol 2022;12:806153. https://doi.org/10.3389/fonc.2022.806153.
[11] Bert C, Durante M. Motion in radiotherapy: particle therapy. Phys Med Biol 2011;56:R113–44. https://doi.org/10.1088/0031-9155/56/16/R01.
[12] Kang Y, Shen J, Liu W, Taylor PA, Mehrens HS, Ding X, et al. Impact of planned dose reporting methods on Gamma pass rates for IROC lung and liver motion phantoms treated with pencil beam scanning protons. Radiat Oncol 2019;14:108. https://doi.org/10.1186/s13014-019-1316-y.
[13] Tryggestad EJ, Liu W, Pepin MD, Hallemeier CL, Sio TT. Managing treatment-related uncertainties in proton beam radiotherapy for gastrointestinal cancers. J Gastrointest Oncol 2020;11:212–24. https://doi.org/10.21037/jgo.2019.11.07.
[14] Gelover E, Deisher AJ, Herman MG, Johnson JE, Kruse JJ, Tryggestad EJ. Clinical implementation of respiratory-gated spot-scanning proton therapy: an efficiency analysis of active motion management. J Appl Clin Med Phys 2019;20:99–108. https://doi.org/10.1002/acm2.12584.
[15] Li H, Dong L, Bert C, Chang J, Flampouri S, Jee K, et al. AAPM Task Group Report 290: Respiratory motion management for particle therapy. Med Phys 2022;49:e50–81. https://doi.org/10.1002/mp.15470.
[16] Yamada T, Takao S, Koyano H, Nihongi H, Fujii Y, Hirayama S, et al. Validation of dose distribution for liver tumors treated with real-time-image gated spot-scanning proton therapy by log data based dose reconstruction. J Radiat Res 2021;62:626–33. https://doi.org/10.1093/jrr/rrab024.
[17] Nakajima K, Iwata H, Ogino H, Hattori Y, Hashimoto S, Toshito T, et al. Clinical outcomes of image-guided proton therapy for histologically confirmed stage I non-small cell lung cancer. Radiat Oncol 2018;13:199. https://doi.org/10.1186/s13014-018-1144-5.
[18] Kulkarni NM, Hong TS, Kambadakone A, Arellano RS. CT-guided implantation of intrahepatic fiducial markers for proton beam therapy of liver lesions: assessment of success rate and complications. Am J Roentgenol 2015;204:W207–13. https://doi.org/10.2214/AJR.14.12901.
[19] Khullar K, Dhawan ST, Nosher J, Jabbour SK. Fiducial marker migration following computed tomography-guided placement in the liver: a case report. AME Case Rep 2021;5. https://doi.org/10.21037/acr-20-153. 15–15.
[20] Dolde K, Naumann P, Dávid C, Kachelriess M, Lomax AJ, Weber DC, et al. Comparing the effectiveness and efficiency of various gating approaches for PBS proton therapy of pancreatic cancer using 4D-MRI datasets. Phys Med Biol 2019;64:085011. https://doi.org/10.1088/1361-6560/ab1175.
[21] Ehrbar S, Perrin R, Peroni M, Bernatowicz K, Parkel T, Pytko I, et al. Respiratory motion-management in stereotactic body radiation therapy for lung cancer – a dosimetric comparison in an anthropomorphic lung phantom (LuCa). Radiother Oncol 2016;121:328–34. https://doi.org/10.1016/j.radonc.2016.10.011.
[22] Ehrbar S, Jöhl A, Tartas A, Stark LS, Riesterer O, Klöck S, et al. ITV, mid-ventilation, gating or couch tracking – a comparison of respiratory motion-management techniques based on 4D dose calculations. Radiother Oncol 2017;124:80–8. https://doi.org/10.1016/j.radonc.2017.05.016.
[23] Nankali S, Worm ES, Thomsen JB, Stick LB, Bertholet J, Høyer M, et al. Intrafraction tumor motion monitoring and dose reconstruction for liver pencil beam scanning proton therapy. Front Oncol 2023;13:1112481. https://doi.org/10.3389/fonc.2023.1112481.
[24] Kostiukhina N, Palmans H, Stock M, Knopf A, Georg D, Knäusl B. Time-resolved dosimetry for validation of 4D dose calculation in PBS proton therapy. Phys Med Biol 2020;65:125015. https://doi.org/10.1088/1361-6560/ab8d79.
[25] Cloutier E, Beaulieu L, Archambault L. Deformable scintillation dosimeter: II. Real-time simultaneous measurements of dose and tracking of deformation vector fields. Phys Med Biol 2021;66:175017. https://doi.org/10.1088/1361-6560/ac1ca2.
[26] Meijers A, Jakobi A, Stützer K, Guterres Marmitt G, Both S, Langendijk JA, et al. Log file-based dose reconstruction and accumulation for 4D adaptive pencil beam scanned proton therapy in a clinical treatment planning system: implementation and proof-of-concept. Med Phys 2019;46:1140–9. https://doi.org/10.1002/mp.13371.
[27] Kostiukhina N, Palmans H, Stock M, Georg D, Knäusl B. Dynamic lung phantom commissioning for 4D dose assessment in proton therapy. Phys Med Biol 2019;64:235001. https://doi.org/10.1088/1361-6560/ab5132.
[28] De Deene Y, Skyt PS, Hil R, Booth JT. FlexyDos3D: a deformable anthropomorphic 3D radiation dosimeter: radiation properties. Phys Med Biol 2015;60:1543–63. https://doi.org/10.1088/0031-9155/60/4/1543.
[29] Høye EM, Skyt PS, Yates ES, Muren LP, Petersen JBB, Balling P. A new dosimeter formulation for deformable 3D dose verification. J Phys Conf Ser 2015;573:012067. https://doi.org/10.1088/1742-6596/573/1/012067.
[30] Maynard E, Heath E, Hilts M, Jirasek A. Introduction of a deformable x-ray CT polymer gel dosimetry system. Phys Med Biol 2018;63:075014. https://doi.org/10.1088/1361-6560/aab501.
[31] Jensen SV, Erichsen TB, Jensen MB, Worm E, Poulsen PR, Petersen JBB, et al. Developing a 3D-printing-based method to create anthropomorphic dosimeters for radiotherapy-delivery verification. J Phys Conf Ser 2023;2630:012038. https://doi.org/10.1088/1742-6596/2630/1/012038.
[32] Høye EM, Sadel M, Kaplan L, Skyt PS, Muren LP, Petersen JBB, et al. First 3D measurements of proton beams in a deformable silicone-based dosimeter. J Phys Conf Ser 2017;847:012021. https://doi.org/10.1088/1742-6596/847/1/012021.
[33] Jensen SV, Valdetaro LB, Poulsen PR, Balling P, Petersen JB, Muren LP. Dose-response of deformable radiochromic dosimeters for spot scanning proton therapy. Phys Imaging Radiat Oncol 2020;16:134–7. https://doi.org/10.1016/j.phro.2020.11.004.
[34] Valdetaro LB, Høye EM, Skyt PS, Petersen JBB, Balling P, Muren LP. Empirical quenching correction in radiochromic silicone-based three-dimensional dosimetry of spot-scanning proton therapy. Phys Imaging Radiat Oncol 2021;18:11–8. https://doi.org/10.1016/j.phro.2021.03.006.
[35] Jensen SV, Muren LP, Balling P, Petersen JB, Valdetaro LB, Poulsen PR. Dose perturbations in proton pencil beam delivery investigated by dynamically deforming silicone-based radiochromic dosimeters. Phys Med Biol 2022;67:235002. https://doi.org/10.1088/1361-6560/ac9fa2.
[36] Ehrbar S, Jöhl A, Kühni M, Meboldt M, Ozkan Elsen E, Tanner C, et al. ELPHA: dynamically deformable liver phantom for real-time motion-adaptive radiotherapy treatments. Med Phys 2019;46:839–50. https://doi.org/10.1002/mp.13359.
[37] Suh Y, Dieterich S, Cho B, Keall P. An analysis of thoracic and abdominal tumour motion for stereotactic body radiotherapy patients. Phys Med Biol 2008;53:3623. https://doi.org/10.1088/0031-9155/53/13/016.
[38] Taasti VT, Høye EM, Hansen DC, Muren LP, Thygesen J, Skyt PS, et al. Technical Note: improving proton stopping power ratio determination for a deformable silicone-based 3D dosimeter using dual energy CT. Med Phys 2016;43:2780–4. https://doi.org/10.1118/1.4948677.
[39] Matenine D, Mascolo-Fortin J, Goussard Y, Després P. Evaluation of the OSC-TV iterative reconstruction algorithm for cone-beam optical CT. Med Phys 2015;42:6376–86. https://doi.org/10.1118/1.4931604.
[40] Worm ES, Hansen R, Høyer M, Weber B, Mortensen H, Poulsen PR. Uniform versus non-uniform dose prescription for proton stereotactic body radiotherapy of liver tumors investigated by extensive motion-including treatment simulations. Phys Med Biol 2021;66:205009. https://doi.org/10.1088/1361-6560/ac2880.
[41] Kanehira T, Matsuura T, Takao S, Matsuzaki Y, Fujii Y, Fujii T, et al. Impact of real-time image gating on spot scanning proton therapy for lung tumors: a simulation study. Int J Radiat Oncol Biol Phys 2017;97:173–81. https://doi.org/10.1016/j.ijrobp.2016.09.027.
[42] Brix L, Ringgaard S, Sørensen T, Poulsen P. Three-dimensional liver motion tracking using real-time two-dimensional MRI. Med Phys 2014;41:042302. https://doi.org/10.1118/1.4867859.
[43] Matrosic CK, Hull J, Palmer B, Culberson W, Bednarz B. Deformable abdominal phantom for the validation of real-time image guidance and deformable dose accumulation. J Appl Clin Med Phys 2019;20:122–33. https://doi.org/10.1002/acm2.12687.
[44] Ribeiro CO, Knopf A, Langendijk JA, Weber DC, Lomax AJ, Zhang Y. Assessment of dosimetric errors induced by deformable image registration methods in 4D pencil beam scanned proton treatment planning for liver tumours. Radiother Oncol 2018;128:174–81. https://doi.org/10.1016/j.radonc.2018.03.001.